ChemComm

COMMUNICATION

View Article Online
View Journal | View Issue

Cite this: *Chem. Commun.*, 2016, 52, 10743

Received 30th May 2016,
Accepted 3rd August 2016

DOI: 10.1039/c6cc04521a

www.rsc.org/chemcomm

Thermally induced recrystallization of $MAPbI_3$ perovskite under methylamine atmosphere: an approach to fabricating large uniform crystalline grains†

Daniel L. Jacobs and Ling Zang*

A liquid to solid phase transition of methylammonium lead triiodide ($MAPbI_3$) under methylamine (MA) atmosphere at elevated temperatures was discovered, and used to form high quality and uniform thin films containing large, low defect crystal grains tens of microns in size.

Hybrid organic–inorganic photovoltaic devices, particularly those based on methylammonium lead triiodide ($MAPbI_3$), have shown unprecedented performance growth in less than a decade, with the most recent record efficiencies above 20%.[1] However, controlling the deposition and crystallization of $MAPbI_3$ has been a significant challenge in reproducibly fabricating high efficiency devices. Early devices were typically fabricated from a simple 1-step spin coating deposition followed by thermal annealing to recrystallize the film. However, these films suffered from large and non-uniform grains due to the fast crystal growth kinetics during the annealing step, which also leads to the formation of significant pinhole area that limit device performance.[2] Major breakthroughs in $MAPbI_3$-based solar cells have stemmed from new deposition techniques capable of forming large area, uniform, smooth and pin hole-free thin films. Such techniques include the 2-step deposition methods,[3,4] anti-solvent methods,[5,6] and the hot casting method.[7] The common underlying mechanism behind the enhanced surface coverage from these techniques is based on increasing the nucleation kinetics during crystallization, which results in small uniform grains across the substrate.[8] However, this comes at the cost of increased grain boundary area, which can also limit the photovoltaic performance. While there have been several techniques developed to increase the grain size through traditional post deposition techniques, such as thermal or solvent annealing, the resulting grains are still typically limited to the micron scale or less.[9,10] The hot casting technique developed by Nie *et al.* has reported ultra large grains up to the millimeter scale,[7] however, subsequent detailed studies of this method suggest that these domains are not single crystals, rather the large area domains are compositions of smaller crystal grains formed in a Volmer–Weber thin film growth process.[11,12] Thus, techniques to fabricate large area single crystal grains uniformly across the surface remains a significant barrier to further improving device performance.

Among the many promising physical properties of organometallic hybrid perovskite materials, the reported room temperature solid to liquid phase transition under methylamine (MA) gas atmosphere is particularly unique. Zhou *et al.* first reported the phenomenon and found that short exposure of a $MAPbI_3$ thin film to MA gas at room temperature causes an immediate color change from dark brown to completely transparent, and when removed from the MA atmosphere, the process quickly reversed.[13] The morphology of the MA treated films show ultra smooth surfaces across the entire sample with enhanced crystallinity leading to improved photovoltaic performance. However, the grain sizes may actually decrease by up to an order of magnitude after exposure to MA.[14] The interaction between MA and $MAPbI_3$ is believed to be a result of polar MA molecules disrupting the ionic bonding of the Pb-I lattice causing a collapse of the crystal structure and forming a $MAPbI_3{\cdot}x$MA liquid phase, with x being estimated at ~ 3.5.[13] When the film is removed from the MA atmosphere, the complex formation quickly reverses as the gas molecules are expelled and $MAPbI_3$ is recrystallized. Compared to a solvent phase crystallization process, which requires the liquid solvent molecules to evaporate before crystallization can occur, the gas phase MA molecules are expelled from the film uniformly and at a much faster rate. This effectively quenches molecular transport, and thereby crystal growth, leading to formation of fine grained thin films dominated by a nucleation process.[8]

In this work, the above reported gas phase annealing process was further investigated at elevated temperatures, 25–100 °C, as shown in Fig. 1. It was found that above 55 °C, the liquid phase of $MAPbI_3$ under MA atmosphere becomes unstable, and starts

Nano Institute of Utah and Department of Materials Science and Engineering, University of Utah, 36 South Wasatch Drive, Salt Lake City, Utah 84112, USA. E-mail: lzang@eng.utah.edu

† Electronic supplementary information (ESI) available: Experimental details, supporting SEM images, supporting video. See DOI: 10.1039/c6cc04521a

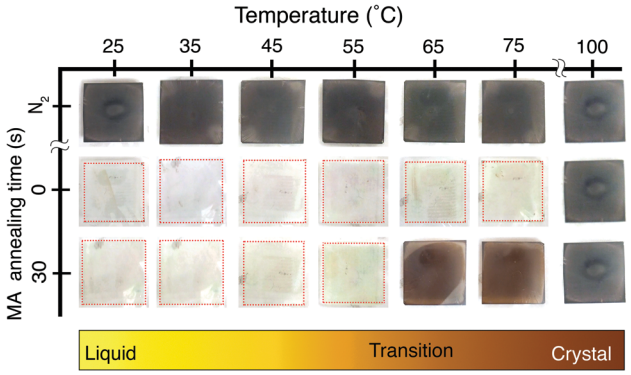

Fig. 1 Temperature dependent annealing of $MAPbI_3$ under MA gas atmosphere. Shown here are the images of seven $MAPbI_3$ coated glass substrates exposed to nitrogen or MA atmosphere maintained at a constant temperature. All images in a column represent the same sample at a constant temperature at different times throughout the experiment. Top row: Images of the as deposited film after five minutes under flowing nitrogen atmosphere at the corresponding temperature. Middle row: Image of the films immediately after exposure to MA atmosphere. Bottom row: Images of the samples after 30 seconds under continual flowing MA atmosphere. The schematic at the bottom shows the proposed 1-D phase diagram of $MAPbI_3$ under a constant MA atmosphere.

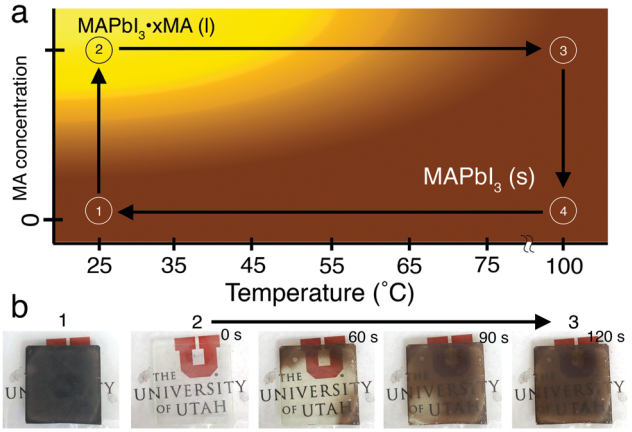

Fig. 2 Experimental procedure of the TIRMA process. (a) Proposed 2-D phase diagram showing the experimental path of TIRMA. (b) *In situ* images of $MAPbI_3$ thin films during the TIRMA process. The $MAPbI_3$ film as prepared in ambient air (25 °C) was an opaque dark brown color (State 1). Immediately after exposure to MA atmosphere at room temperature, the film transformed to a colorless liquid state (State 2). The film (after exposed to MA for 30 s) was heated up to 100 °C, and during the 120 s heating it started to recrystallize, eventually forming the crystalline phase with a semi-transparent brown color (State 3). After complete recrystallization, the MA atmosphere was purged with nitrogen for 2 minutes at 100 °C (State 4) followed by cooling to room temperature to form the final state. No significant difference after State 3 through the final state was found regarding either structure or morphology.

transitioning back to the solid state. At 100 °C, no liquid intermediate phase exists. This liquid–solid phase transition at higher temperatures, as illustrated in the one-dimensional (1-D) phase diagram (Fig. 1), is similar to the inverse temperature crystallization phenomenon as observed in solution phase for many of the organo-metallic halide perovskites. For example, $MAPbI_3$ can precipitate out of a heated solution in γ-butyrolacetone, which can be used to rapidly grow large single crystals through controlled heating of the solution.[15] Following a similar approach, high quality and uniform large area thin films of $MAPbI_3$ with large, highly crystalline grains were formed from the thermally induced recrystallization under methylamine atmosphere (TIRMA) process introduced herein.

$MAPbI_3$ films were prepared in air on glass substrates *via* a 1-step spin coating with antisolvent drip technique.[6] The experimental path of the TIRMA process related to changes in the substrate temperature and the gas atmosphere is shown on the 2-D phase diagram in Fig. 2a. Fig. 2b shows snapshots of the $MAPbI_3$ films during TIRMA treatment and a full video can be found in the ESI.† Samples were loaded into a sealed homemade chamber at room temperature and purged with nitrogen for 5 minutes. MA gas was introduced by routing the nitrogen flow to a sealed 100 mL flask containing 5 mL of a 33 wt% solution of MA in ethanol to carry the headspace gas to the sample chamber. After being exposed to MA, the opaque dark brown $MAPbI_3$ film was immediately transitioned into the transparent colorless liquid state of $MAPbI_3{\cdot}x$MA. After 30 s under constant MA atmosphere, the chamber was placed on a hot plate preheated to 100 °C. Upon heating, the film began to recrystallize, initially from the edges, followed by massive growth throughout the film until complete recrystallization occurred. When the recrystallization was complete, the system was switched back to the nitrogen atmosphere and kept on the hot plate for 2 minutes. Finally, the chamber was removed from the hotplate and cooled to room temperature. No structural or morphology change of the $MAPbI_3$ film was observed during the nitrogen purge or the cooling steps. Detailed experimental methods can be found in the ESI.†

The TIRMA process resulted in exceptional film coverage and film quality as summarized in Fig. 3. The grain sizes of the TIRMA treated samples increased by about 2 orders of magnitude compared with the pristine film (Fig. 3a, a high magnification SEM image in Fig. S1 (ESI†), and cross sectional SEM image in Fig. S2, ESI†) with an average grain size of the TIRMA treated film estimated to be about 15 μm (Fig. 3b). The SEM image of the TIRMA treated sample in Fig. 3b shows a highly crystalline morphology with crystal twin boundaries clearly observed. The sample showed uniform morphology across the surface and no significant pin-holing was observed as evidenced by the cross sectional SEM image (Fig. 3c) and large area SEM image (Fig. S3, ESI†) (a note on the observed dark lines in the SEM images of the TIRMA sample is provided in the ESI†). The enhanced crystallinity of the film is supported by X-ray diffraction (XRD) studies. As seen in Fig. 3d, the pristine $MAPbI_3$ film showed mostly (110) lattice orientation in addition to several minority orientations. However, the TIRMA treated samples showed an increase in the peak intensity by over 2 orders of magnitude with strong preferred lattice orientation only in the (110) direction. The full width half max (FWHM) of the (110) reflection at 14° decreased 36% from 0.106° to 0.068°, signifying a significant increase in grain size. To further show the improved crystallinity and phase purity of the TIRMA treated samples, photoluminescence (PL) spectral measurement was performed for the $MAPbI_3$ film before and after TIRMA treatment (Fig. 3e). The TIRMA treated sample

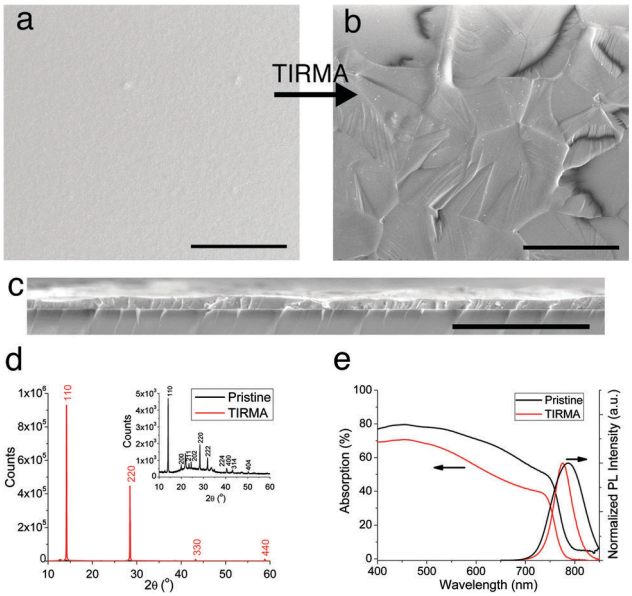

Fig. 3 SEM image of (a) pristine and (b) TIRMA treated $MAPbI_3$ showing the formation of large crystalline grains (scale bars are 20 μm). (c) Cross sectional SEM image of TIRMA treated film (scale bar is 3 μm). Cross sectional SEM image of the pristine film is shown in Fig. S2 (ESI†) for comparison. (d) XRD spectra of a pristine and a TIRMA treated $MAPbI_3$ film. The inset shows the isolated pristine $MAPbI_3$ film spectrum for comparison. (e) Absolute absorption and normalized photoluminescence spectra of a pristine and a TIRMA treated $MAPbI_3$ film.

showed a 10 nm blue shift of the PL peak from 785 to 775, and a decrease in the FWHM from 74 nm to 46 nm, indicating a reduction of low lying bulk and grain boundary defects.[10,14,16] This PL peak shift is accompanied with a blue shift of the absorption band edge seen in the absorption spectrum in Fig. 3e. Tauc plot (Fig. S5, ESI†) shows the band edge shifting from 1.59 eV for the pristine film to 1.62 eV for the TIRMA treated sample, which converts to about a 15 nm shift, similar to the PL shifting. The absorption spectra in Fig. 3e show a decrease in the overall absorption after TIRMA treatment. This correlates with the apparent increase in transmission during the TIRMA process visible in the ESI,† movie and in Fig. 2b, which is attributed to the significant change in grain size. The pristine film contains grain sizes on the order of the wavelength of visible light, and should therefore be more efficient in scattering the light within the film, resulting in an increase in the optical path length. In comparison, the TIRMA treated films have grains over an order of magnitude larger than the wavelength of incident light, which should decrease light scattering and therefore the path length of light within the film.

For comparison, the fast annealing technique in MA vapor at room temperature (MA_{RT}) used in previously reported studies[13,14] was performed and characterized. In short, the as-deposited film was brought into the headspace of a vial containing the MA solution at room temperature for a short amount of time (~1 s), and rapidly brought back into air. The MA_{RT} treated film was characterized using UV-vis absorption and PL spectra, SEM imaging, and XRD as shown in Fig. S6 (ESI†). The MA_{RT} treatment did not result in any significant change in grain size compared to the pristine sample, but did cause observable morphology change with the MA_{RT} film showing less defined and distinct grain boundaries. This implies that MA_{RT} treatment helps to heal grain boundary defects. The XRD measurement supports this with a drastic increase (2 orders of magnitude) in the peak intensity and much more uniform crystal orientation compared to the pristine film. The FWHM was calculated to be 0.093° for the MA_{RT} film, similar to the pristine, which supports the observation of no significant change in grain size. The UV-vis absorption and PL spectra also show a similar trend to the TIRMA films, with the PL showing a decrease in FWHM to 48.5 nm and a blue shift in the absorption band edge to about 1.6 eV. While the MA_{RT} film shows significant improvement in the film quality compared to the pristine films, it is less than what is achieved with the TIRMA treatment regarding the grain size and crystallinity.

The unprecedented enhancement in crystallinity of the TIRMA treated $MAPbI_3$ film is proposed to be a result of the slow growth controlled crystallization as opposed to the fast nucleation driven process. Fig. 4 shows a schematic of the proposed mechanism of the TIRMA process. When the $MAPbI_3$ is exposed to the MA gas at room temperature, the colorless liquid phase $MAPbI_3{\cdot}xMA$ is immediately formed. When the chamber is put on the hot plate, a vertical temperature gradient is created up through the $MAPbI_3$ film. As the substrate temperature reaches the critical temperature (>55 °C), the colorless liquid phase begins to show a darker yellow color as seen in Fig. 2b at 60 s and the ESI,† Video. This yellow color can also be seen in images in Fig. 1, particularly at 55 °C, 65 °C and 75 °C samples. This yellow film is proposed to be an intermediate phase, $MAPbI_3{\cdot}(x–y)MA$, resulted from the partial expulsion of MA molecules from the room temperature equilibrium state $MAPbI_3{\cdot}xMA$. The equilibrium molar ratio $(x–y)$ depends on the temperature, and more work is needed to characterize this

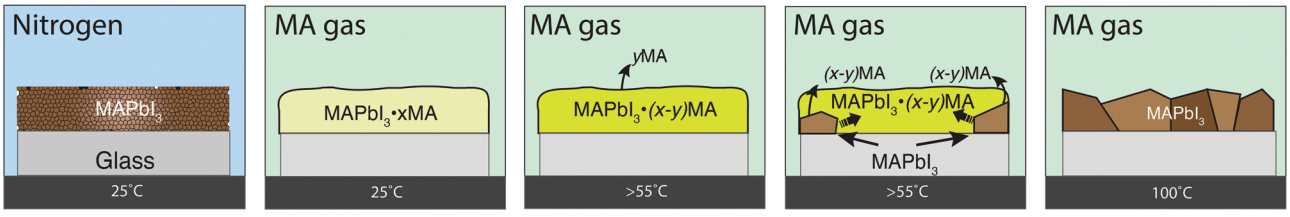

Fig. 4 Schematic of proposed TIRMA mechanism leading to large crystalline grain film. (a) As deposited $MAPbI_3$ film under nitrogen at room temperature. (b) Exposure to MA at room temperature leading to $MAPbI_3{\cdot}xMA$ liquid phase. (c) Increasing substrate temperature leading to partial expulsion of MA molecules. (d) Nucleation of $MAPbI_3$ at the film edge followed by crystal growth *via* cellular precipitation as more MA molecules are expulsed from the film. (e) Stable crystalline phase reached when all excessive MA molecules are released from the film.

intermediate state. When the substrate temperature rises above the critical temperature, continued expulsion of MA molecules leads to supersaturation, causing $MAPbI_3$ to nucleate on the surface. By maintaining a constant elevated temperature throughout the process, the $MAPbI_3$ nuclei grow by continuous expulsion of MA. Such phase growth process can be considered as a typical case of cellular precipitation, $\gamma \rightarrow \alpha + \beta$, where the γ represents the liquid phase of $MAPbI_3{\cdot}(x–y)MA$, α represents the solid precipitate of $MAPbI_3$, and β is the gas phase of MA. As the whole system remains in the MA atmosphere, the α and β are in equilibrium, *i.e.*, precipitation of $MAPbI_3$ and release of MA gas occur simultaneously at the expense of the original supersaturated phase of $MAPbI_3{\cdot}(x–y)MA$. The diffusion distance remained short and unchanged during the phase growth process as seen from the approximately constant moving rate of the recrystallization front in the video in the ESI.† Because the precipitation of $MAPbI_3$ is driven by expulsion of MA gas, the phase transition occurs at higher temperature, reverse to the other cellular precipitation processes, which are usually triggered by decreasing temperatures.

In conclusion, a liquid–solid phase transition of $MAPbI_3{\cdot}x$MA into $MAPbI_3$ at elevated temperatures was revealed under constant MA gas atmosphere. This phenomenon was used to directly crystallize $MAPbI_3$ thin film with crystal grains on the order of tens of micrometers. The resultant film showed significantly enhanced crystallinity and reduced bulk crystal defects. This TIRMA process can be interpreted as a typical cellular precipitation, which allows for kinetic control (*via* temperature) of the phase growth in order to form large uniform crystalline domains with minimal defects. The films thus formed also afford complete and compact coverage across the substrate. Future studies to control the nucleation and growth kinetics through more precise control of temperature and MA concentration, along with appropriate surface modification of the substrate is anticipated to further increase the size and quality of crystal grains and the uniformness of the film, which combined will facilitate the fabrication of high efficiency photovoltaic devices.

This work was supported by the University of Utah Seed Grant and the State of Utah USTAR Program. D. L. J. acknowledges support from the NSF IGERT (DGE0903715). The Authors would like to acknowledge Michael A. Scarpulla for his helpful discussions.

Notes and references

1 M. Saliba, T. Matsui, J.-Y. Seo, K. Domanski, J.-P. Correa-Baena, M. K. Nazeeruddin, S. M. Zakeeruddin, W. Tress, A. Abate, A. Hagfeldt and M. Gratzel, *Energy Environ. Sci.*, 2016, **9**, 1989–1997.
2 G. E. Eperon, V. M. Burlakov, P. Docampo, A. Goriely and H. J. Snaith, *Adv. Funct. Mater.*, 2014, **24**, 151–157.
3 Q. Chen, H. Zhou, Z. Hong, S. Luo, H. S. Duan, H. H. Wang, Y. Liu, G. Li and Y. Yang, *J. Am. Chem. Soc.*, 2014, **136**, 622–625.
4 J. Burschka, N. Pellet, S. J. Moon, R. Humphry-Baker, P. Gao, M. K. Nazeeruddin and M. Gratzel, *Nature*, 2013, **499**, 316–319.
5 N. J. Jeon, J. H. Noh, Y. C. Kim, W. S. Yang, S. Ryu and S. I. Seok, *Nat. Mater.*, 2014, **13**, 897–903.
6 M. Xiao, F. Huang, W. Huang, Y. Dkhissi, Y. Zhu, J. Etheridge, A. Gray-Weale, U. Bach, Y.-B. Cheng and L. Spiccia, *Angew. Chem., Int. Ed.*, 2014, **53**, 9898–9903.
7 W. Nie, H. Tsai, R. Asadpour, J.-C. Blancon, A. J. Neukirch, G. Gupta, J. J. Crochet, M. Chhowalla, S. Tretiak, M. A. Alam, H.-L. Wang and A. D. Mohite, *Science*, 2015, **347**, 522–525.
8 Y. Zhou, O. S. Game, S. Pang and N. P. Padture, *J. Phys. Chem. Lett.*, 2015, **6**, 4827–4839.
9 Z. Xiao, Q. Dong, C. Bi, Y. Shao, Y. Yuan and J. Huang, *Adv. Mater.*, 2014, **26**, 6503–6509.
10 C. Bi, Q. Wang, Y. Shao, Y. Yuan, Z. Xiao and J. Huang, *Nat. Commun.*, 2015, **6**, 7747.
11 Y. C. Zheng, S. Yang, X. Chen, Y. Chen, Y. Hou and H. G. Yang, *Chem. Mater.*, 2015, **27**, 5116–5121.
12 Y. Deng, E. Peng, Y. Shao, Z. Xiao, Q. Dong and J. Huang, *Energy Environ. Sci.*, 2015, **8**, 1544–1550.
13 Z. Zhou, Z. Wang, Y. Zhou, S. Pang, D. Wang, H. Xu, Z. Liu, N. P. Padture and G. Cui, *Angew. Chem., Int. Ed.*, 2015, **54**, 9705–9709.
14 T. Zhao, S. T. Williams, C.-C. Chueh, D. W. deQuilettes, P.-W. Liang, D. S. Ginger and A. K. Y. Jen, *RSC Adv.*, 2016, **6**, 27475–27484.
15 M. I. Saidaminov, A. L. Abdelhady, B. Murali, E. Alarousu, V. M. Burlakov, W. Peng, I. Dursun, L. Wang, Y. He, G. Maculan, A. Goriely, T. Wu, O. F. Mohammed and O. M. Bakr, *Nat. Commun.*, 2015, **6**, 7586.
16 Y. Shao, Z. Xiao, C. Bi, Y. Yuan and J. Huang, *Nat. Commun.*, 2014, **5**, 5784.

